

Intertwined birth and death: a Herbig–Haro outflow resolves the distance to Vela Junior

JANETTE SUHERLI ¹, IVO R. SEITENZAHL ^{2,3}, SAMAR SAFI-HARB ¹, FRÉDÉRIC P. A. VOGT ⁴, WYNN C. G. HO ⁵,
PARVIZ GHAVAMIAN ⁶, CHUAN-JUI LI ⁷, ASHLEY J. RUITER ², ROLAND M. CROCKER ³, ARPITA ROY ³, AND
RALPH SUTHERLAND ³

¹ *University of Manitoba, Department of Physics and Astronomy*

² *Australian National University, Mathematical Sciences Institute*

³ *Australian National University, Research School of Astronomy and Astrophysics*

⁴ *Federal Office of Meteorology and Climatology MeteoSwiss*

⁵ *Department of Physics and Astronomy, Haverford College, 370 Lancaster Avenue, Haverford, PA 19041, USA*

⁶ *Towson University, Department of Physics, Astronomy and Geosciences*

⁷ *National Chengchi University, Graduate Institute of Applied Physics*

ABSTRACT

The distance to the Vela Junior supernova remnant (RX J0852.0–4622 or G266.2–1.2) has long remained uncertain, limiting our understanding of its physical properties. Using VLT/MUSE integral field spectroscopy, we uncover chemical and kinematic connections between the nebula surrounding its Central Compact Object (CXOU J085201.4–461753) and the nearby Herbig-Haro outflow of Ve 7–27 (Wray 16–30), indicating a shared nitrogen-rich, Fe-peak-enhanced environment. This link ties stellar birth and death, with the young star Ve 7–27 embedded in material expelled by Vela Junior’s massive progenitor, and the remnant’s blast wave is expanding through the same medium. Adopting the *Gaia*-based distance to Ve 7–27, we revise Vela Junior’s distance to 1.41 ± 0.14 kpc. At this distance, the remnant’s physical radius is 23.3 ± 2.3 pc, and X-ray proper motions of the northwestern rim correspond to shock speeds of $(2.8 \pm 0.7) \times 10^3$ to $(5.6 \pm 1.5) \times 10^3$ km s^{−1}. These imply an age of ~ 1.6 – 3.3 kyr and a very low ambient density, indicating that Vela Junior is expanding within a highly rarefied wind-blown cavity carved by a massive progenitor – consistent with the non-detection of strong thermal X-ray emission. This distance update also resolves long-standing inconsistencies, with major implications for its energy budget, particle acceleration efficiency, and compact object evolution.

Keywords: Supernova remnants (1667) — Compact nebulae (287) — Herbig-Haro objects (722)

1. INTRODUCTION

Massive stars and their deaths both seed and sculpt galaxies: they form in dense molecular clouds, enrich the interstellar medium (ISM) through their winds, and end their lives as supernovae that inject energy and heavy elements, drive fast shocks, and accelerate cosmic rays. Supernova remnants (SNRs) are therefore prime laboratories for studying these processes. However, interpretations are often limited by uncertain distance estimates, which set the fundamental scale for ages, energetics, and particle acceleration.

Vela Junior (RX J0852.0–4622, G266.2–1.2, hereafter Vela Jr) exemplifies this problem. Despite more than two decades of study, its distance has remained remark-

ably uncertain, with published estimates spanning over an order of magnitude (Figure 1; see Appendix A). This wide spread has led to mutually inconsistent inferences for its intrinsic properties. Early work suggested that Vela Jr is an exceptionally nearby and young remnant, whereas later analyses based on X-ray absorption modeling, shock proper-motions, and the properties of its central compact object (CCO) favored substantially larger distances. All of these estimates, however, are inherently model-dependent and often probe only the northwestern rim.

Discovered in *ROSAT* hard X-ray data in 1998 (Aschenbach 1998), Vela Jr is one of the few synchrotron-dominated SNRs (Slane et al. 2001; Reynolds 2008; Ferland & Safi-Harb 2012) and a prominent TeV γ -ray source (Aharonian et al. 2005, 2007; H. E. S. S. Collaboration et al. 2018). It has been proposed as a nearby

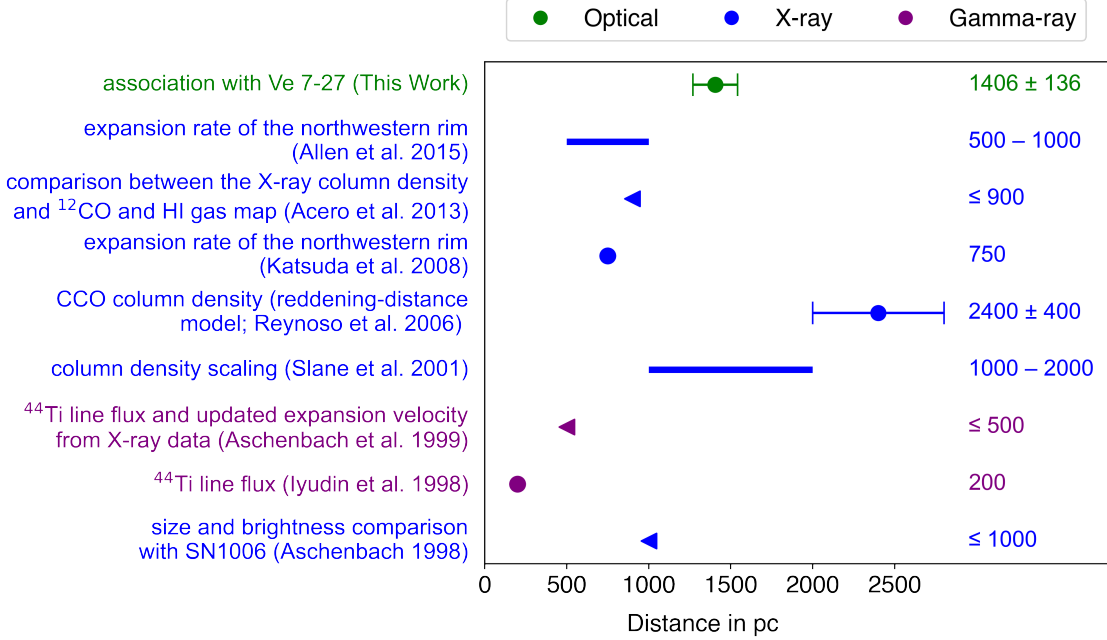


Figure 1. Distance estimates to Vela Jr from the literature (see Appendix A) and this work, arranged in reverse chronological order. The y-axis lists the methods used, and the colors indicate the wavelength regime of the observations used in the estimate: green for optical, blue for X-ray, and purple for γ -ray.

cosmic-ray accelerator (Fukui et al. 2017, 2024) and a potential continuous gravitational-wave emitter (Abbott et al. 2022; Ming et al. 2024). Pinning down its distance accurately is therefore essential not only for interpreting Vela Jr’s properties, but also for constraining models of stellar evolution, particle acceleration, nucleosynthesis, and feedback in the ISM.

Vela Jr hosts the CCO CXOU J085201.4–461753 (Slane et al. 2001; Pavlov et al. 2001), the only CCO known with a detected optical nebula (Pellizzoni et al. 2002; Mignani et al. 2007; Suherli et al. 2024). CCOs, typified by the one in Cas A (Tananbaum 1999), form a rare class of young neutron stars that emit almost exclusively in the soft X-ray band and lack observable pulsar wind nebulae, radio pulsations, or γ -ray emission (De Luca 2017). The optical nebula surrounding the Vela Jr CCO was initially identified as an $\text{H}\alpha$ nebula, possibly a bow shock or photoionized cloud (Pellizzoni et al. 2002; Mignani et al. 2007). MUSE observations revealed it to be $8''$ wide, dominated by $[\text{N II}]\lambda\lambda 6548, 6583$ emission (Suherli et al. 2024), with a faint, previously undetected arc of $\text{H}\alpha$ along its southern edge. Photoionization modeling shows the nebula is consistent with nitrogen-rich gas illuminated by a hot source consistent with the CCO thermal radiation. The extreme nitrogen ($[\text{N II}]\lambda\lambda 6548+6583/\text{H}\alpha \sim 34$) composition of the gas matches the expectations from the final wind phase of a massive nitrogen-rich Wolf-Rayet (WN) star (Roy et al.

2020). This fossil wind, now lit by the CCO, indicates that Vela Jr formed from the collapse of a WN-type star that shed much of its outer layers before the supernova, enriching its surroundings with stellar material.

In this Letter, we present the Multi Unit Spectroscopic Explorer (MUSE; Bacon et al. 2010) observations of the central region of Vela Jr (Program ID 0104.D-0092(B); P.I.: F.P.A. Vogt; see Appendix B), covering both the CCO nebula and the bright emission object Ve 7–27¹ (Wray 16–30), located $\sim 22''$ from the CCO. The full MUSE mosaic provides a comprehensive view of the CCO nebula and Ve 7–27, including its bipolar outflow and its interaction with the surrounding nitrogen-enriched medium. In Section 2, we show that Ve 7–27 is a Herbig-Haro object with pronounced nitrogen enrichment and in Section 3, we demonstrate the chemical and kinematic associations between Ve 7–27 and the CCO nebula, which enables a revised, model-independent distance to Vela Jr. Section 4 discusses the implications of this new distance for the remnant’s physical parameters and the broader evolutionary context of the system, and Section 5 summarizes our conclusions.

¹ Sometimes listed erroneously as Ve 2–27.

2. VE 7–27: A HERBIG-HARO OUTFLOW

Ve 7–27 is a bright emission-line source with a *Gaia* parallax distance of 1406 ± 136 pc (Gaia Collaboration et al. 2021). Its classification has been debated: initially identified as a compact planetary nebula (PN) candidate (Velghe 1957), later reclassified as a Be star (Wray 1966) with near-infrared excess (Allen & Glass 1975), and subsequently reported to show low-ionization optical spectral features reminiscent of η Carinae² (Landaberry et al. 2001). Such spectra indicate dense circumstellar material, but are not uniquely diagnostic of the underlying stellar type. Follow-up radio observations again favored the PN interpretation (Reynoso et al. 2006).

MUSE provides the first spatially resolved view of Ve 7–27’s optical structure, revealing features inconsistent with those of a typical PN. Figure 2 shows an RGB composite of H α (R), [N II] λ 6583 (G), and [N II] λ 7378 (B), integrated from -150 km s $^{-1}$ to $+200$ km s $^{-1}$ and rotated so that the jet axis aligns with the y-axis. Ve 7–27 displays a narrow bipolar jet composed of well-defined strings of shock-excited knots. Distinct bow shock structures are observed particularly along the southern jet, while the northern jet is enclosed by a conical cocoon of gas. The bipolar jet extends at least $\sim 47''$ on each side, corresponding to a projected physical length of 0.32 pc. This morphology is characteristic of Herbig-Haro (HH) objects, which trace highly collimated outflows driven by dense shock interactions in the immediate environment of young stellar objects (YSOs) (for reviews, see e.g. Reipurth & Bally 2001; Bally 2016).

The spatial distribution of individual emission lines is shown in Figure 3. The jet knots exhibit the low-ionization emission ([N I], [N II], [S II], and [Fe II]) that trace shock-excited gas arising from ambient material swept up and shocked by the jet, along with unusually strong Fe-peak emission ([Cr II] and [Ni II]) that points to an enriched environment. Along the outflow, the shocked knots show exceptionally strong [N II] emission with notably no oxygen emission, whereas the central source of Ve 7–27 itself exhibits [N II]/H α < 1 , indicating that the enrichment does not originate from the proto-star or its natal cloud, but the environment that the jet is interacting with. The [N II]/H α and [N II]/[S II] maps (Figure 4b and c) provide sensitive diagnostics of nitrogen enrichment and show consistently elevated values throughout both lobes of Ve 7–27. The northern cocoon is traced by Balmer and Paschen lines, [N I], [N II], [S II], [Ca II], and [Fe II], while an extended hourglass-shaped

nebula, shines particularly in [Ni II] and [Cr II], overlaps both lobes and outlines part of the western boundary of the northern cocoon.

A velocity map derived from multi-component fits to the [N II] λ 6548,6583 lines (see Appendix C) in Figure 4a shows a symmetric velocity gradient, with knot D in the northern lobe reaching ~ -50 km s $^{-1}$ and the southernmost knot (knot A) reaching $\sim +50$ km s $^{-1}$. These velocities indicate a bipolar outflow, with one lobe approaching and the other receding, viewed at a moderate inclination to the line of sight. The spatial map of the density-sensitive [S II] λ 6716/ λ 6731 ratio (Figure 4d) shows that only a very compact region immediately surrounding the central source of Ve 7–27 exhibits high electron densities, with ratios $\lesssim 0.5$ corresponding to $n_e \gtrsim 10^4$ cm $^{-3}$ (for $T \approx 10^4$ K). Outside this core, the ratios span 0.9–1.6, which corresponds to low-to-moderate densities of $n_e \lesssim 500$ cm $^{-3}$ under typical nebular temperatures).

The observed collimated outflow, bipolar jet geometry, and shock-excited knots with bow shocks unambiguously point to Ve 7–27 as the driving source of a bipolar HH outflow.

3. REVISED DISTANCE TO VELA JR VIA VE 7–27

Both the outflow of Ve 7–27 and the CCO nebula show emission characteristics that are not expected in normal interstellar or circumstellar environments. In classical HH objects, where jets propagate into molecular cloud material, shocks typically yield [N II]/H α < 1 across a wide range of shock velocities and densities (e.g. Raga et al. 1996; Dopita & Sutherland 2017). However, the HH-shock of Ve 7–27 shows [N II]/H α values reaching ~ 7 (Figure 4b), comparable to the extreme nitrogen enhancement observed in the CCO nebula. These values cannot be generated by shocks propagating into standard ISM compositions and indicate that the ambient gas is unusually nitrogen-rich.

To probe the nature of the nitrogen enrichment, we computed slow-shock models with MAPPINGS v5.2.0 (see Appendix D for details). Figure 5 compares MUSE measurements with the model predictions in the standard diagnostic plane of [S II] λ 6761/ λ 6731 versus [N II]/[S II] λ 6716+ λ 6731. Shock grids assuming standard ISM abundances (Local Galactic Concordance; LGC; Nicholls et al. 2017) fail to reproduce the observed [N II]/[S II] ratios for any combinations of shock velocities and pre-shock densities. In contrast, the observed values are well matched by models adopting nitrogen-enriched, WN-like abundances, identical to those used in Suherli et al. (2024) to model the photoionized CCO nebula. A complementary comparison using the [N II]/H α ratio is

² η Carinae is a Luminous Blue Variable (LBV) object.

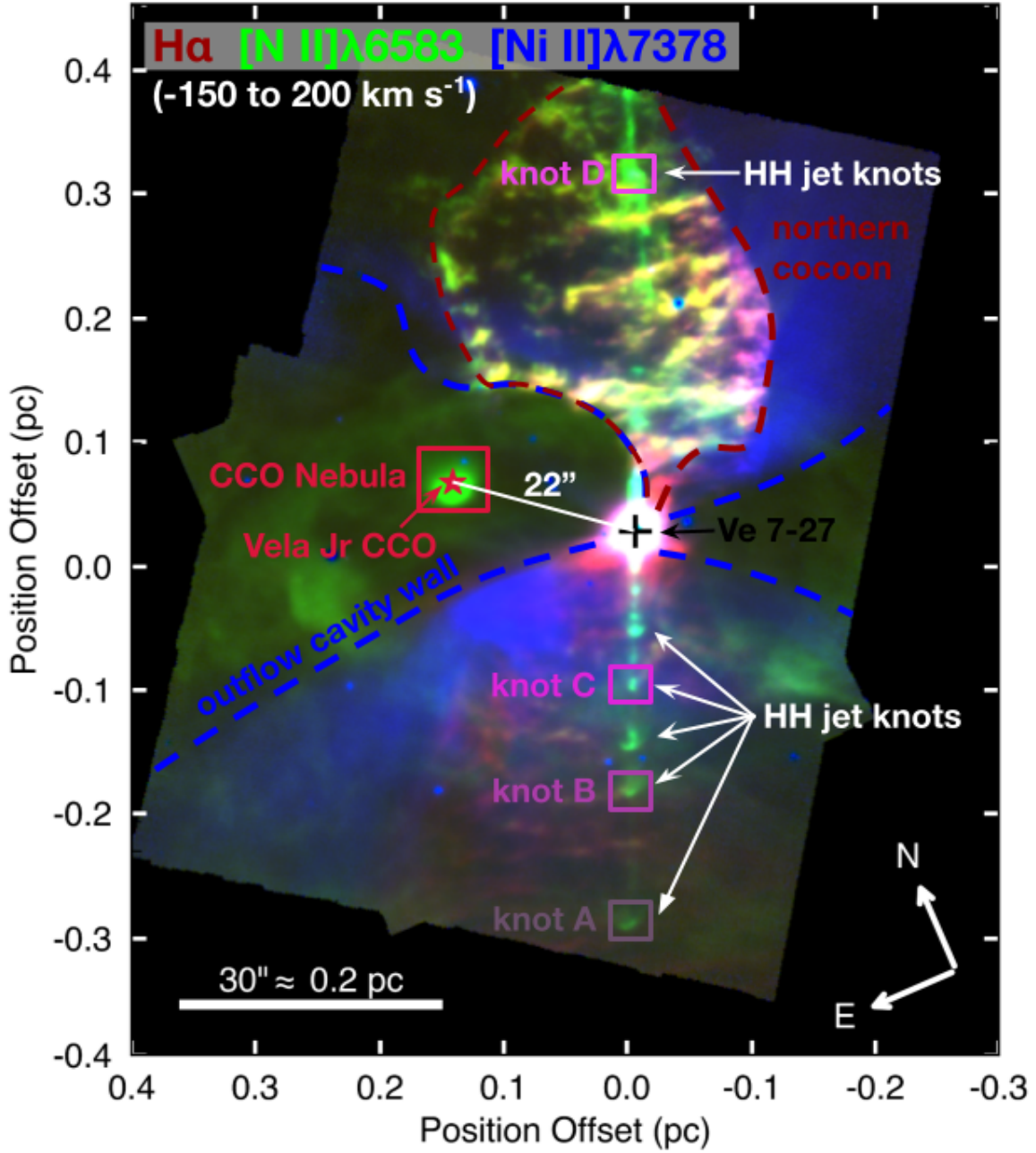


Figure 2. Continuum-subtracted MUSE RGB composite of the central region of Vela Jr in H α (R), [N II] λ 6583 (G), and [Ni II] λ 7378 (B), integrated from -150 km s^{-1} to $+200 \text{ km s}^{-1}$. The image is rotated by 23.5° counter-clockwise to place the jet axis vertically. Key structure of the Ve 7–27 HH system are annotated.

provided in Appendix D (Figure 7); although it is not a standard diagnostic diagram, it independently shows that the Ve 7–27 knots and the CCO nebula cannot be produced by shocks into gas of near ISM-composition.

The optical forbidden lines of Fe-peak elements ([Cr II], [Fe II], and [Ni II]) are rare or completely absent in typical HH objects, which usually show only infrared [Fe II] emission (e.g. at $1.64 \mu\text{m}$). This is because young stellar environments, the protostars themselves and their surrounding molecular clouds, contain negli-

gible gas-phase Fe-peak material, and protostars do not synthesize Fe-peak nuclei. Fe-peak elements are produced primarily in Type Ia supernovae or during the late evolutionary stages of massive stars, and they are released into the surrounding gas through supernova ejecta. Their strong presence in both Ve 7–27 and the CCO nebula (where [Fe II] emission is prominent) indicates that the gas being shocked by the Ve 7–27 jet is chemically pre-enriched, consistent with the ejecta of

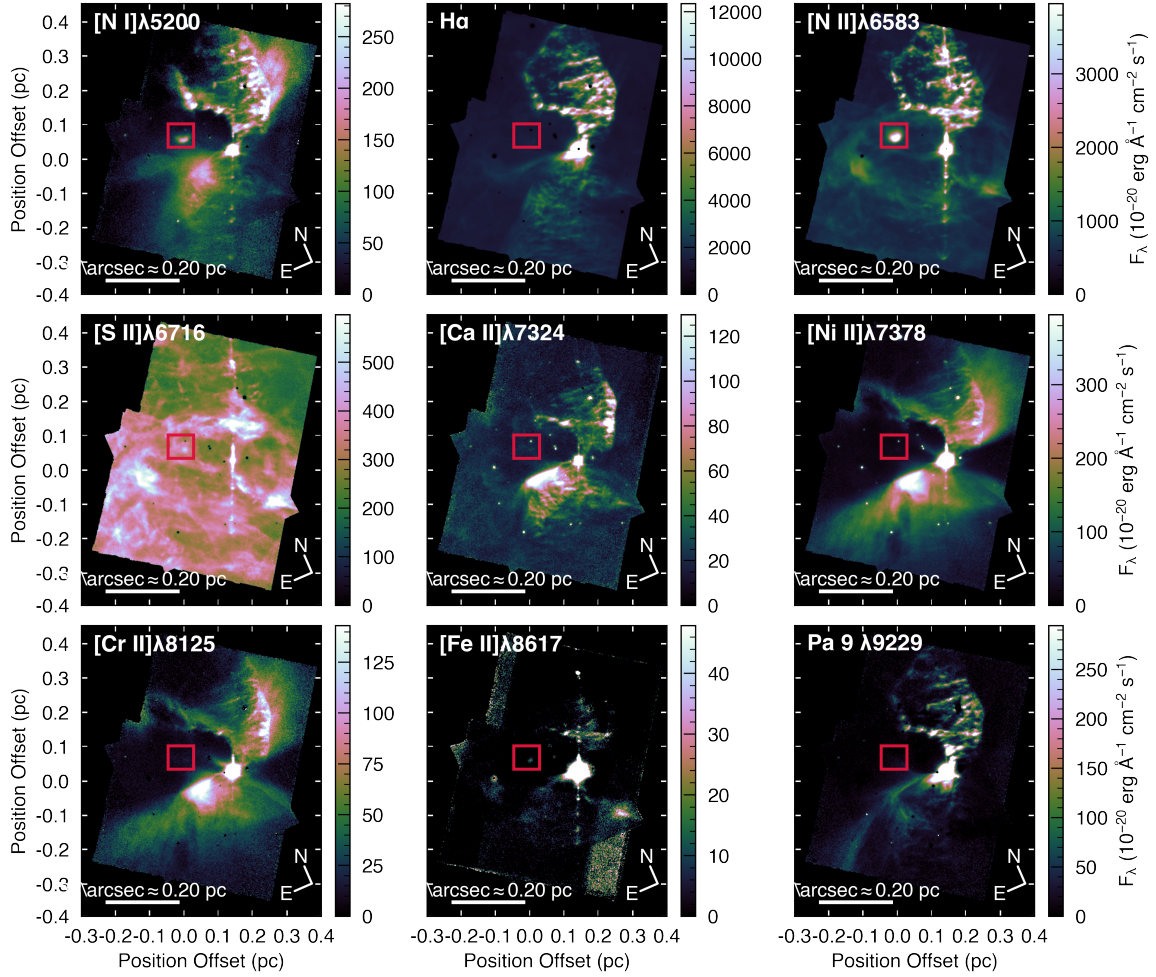


Figure 3. Continuum-subtracted MUSE narrow-band images constructed by integrating each line over the velocity range -150 km s^{-1} to $+200 \text{ km s}^{-1}$. Top row: $[\text{N II}]\lambda 5200$, $\text{H}\alpha$, and $[\text{N II}]\lambda 6583$ line emissions. Middle row: $[\text{S II}]\lambda 6716$, $[\text{Ca II}]\lambda 7324$, and $[\text{Ni II}]\lambda 7378$. Bottom row $[\text{Cr II}]\lambda 8125$, $[\text{Fe II}]\lambda 8617$, and $\text{Pa } 9 \lambda 9229$. The red square in each panel marks the position of Vela Jr CCO nebula.

a massive progenitor rather than gas associated with a standard protostellar environment.

The bright northern cocoon of Ve 7–27 shows a clear geometric distortion along its eastern wall near the base of the outflow, precisely toward where the Vela Jr CCO nebula is. Such deformation is not expected from the internal dynamics of an isolated HH flow, where in the absence of external forces or strong ambient gradients, the outflow maintain approximate symmetry about the flow axis (Reipurth & Bally 2001). The same asymmetry appears in the Fe-peak hourglass shape traced by $[\text{Ni II}]$ and $[\text{Cr II}]$, whose northern lobe bends on the east side whereas the southern counterpart remains symmetric. This directional curvature seen across multiple emission lines indicates that an external influence, rather than intrinsic jet dynamics, is affecting the cocoon’s geometry.

Velocity channel maps constructed from $\text{H}\alpha$ (red), $[\text{N II}]\lambda 6583$ (green), and $[\text{Ni II}]\lambda 7378$ (blue) show that

emission from Ve 7–27 and from the CCO nebula occupies the same spatial regions across a continuous sequence of velocity slices from -150 km s^{-1} to $+200 \text{ km s}^{-1}$ (Figure 6). The two objects do not appear as disjoint velocity structures, nor as unrelated components that overlap only in isolated bins, which is fully consistent with the $[\text{N II}]$ velocity map (Figure 4a), which shows that the HH knots and the CCO nebula span the same range of line-of-sight velocities. This spatial–kinematic continuity reinforces that both systems lie within the same physical volume of enriched gas, rather than being unrelated structures aligned by chance along the line of sight.

The combination of unusually strong nitrogen enrichment, shared morphology, and matched kinematics reveals more than a mere spatial coincidence between Ve 7–27 and the CCO nebula. The chemical signature of the WN-progenitor wind (enhanced nitrogen and de-

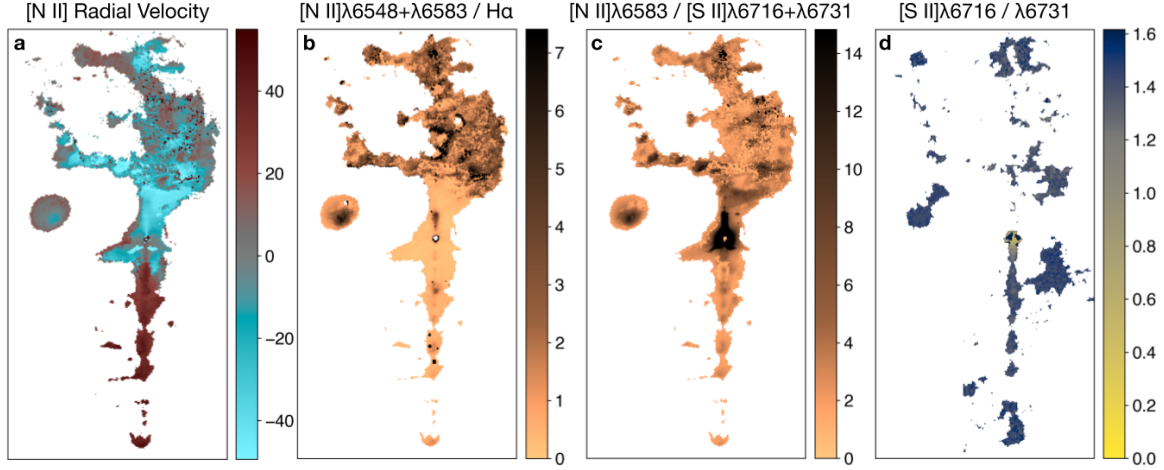


Figure 4. (a) Velocity map of the $[\text{N II}]\lambda 6583$ line, showing the kinematic structure of Ve 7–27 and Vela Jr CCO nebula. (b) Spatial distribution of $[\text{N II}]/\text{H}\alpha$ ratio and (c) $[\text{N II}]/[\text{S II}]$, both highlighting the strong nitrogen enrichment of both Ve 7–27 and the CCO nebula. (d) Spatial map of the canonical electron-density-sensitive $[\text{S II}]\lambda 6716/\lambda 6731$ ratio across the field. This ratio decreases with increasing electron density.

pleted oxygen) imprinted on both objects links them to the same local environment, while the presence of Fe-peak forbidden lines indicates additional contribution from supernova ejecta. These results show that the Ve 7–27 jets are not plowing into ordinary ISM material, but into chemically processed material shed by the progenitor of Vela Jr. The nitrogen-rich environment naturally accounts for the unusually high line ratios and highlights the unique nature of this system: an HH object interacting not with diffuse ISM, but with the enriched wind and ejecta of a dead massive star. Such an association has not been observed before, marking Ve 7–27 as an anomalously enriched HH object whose emission properties are directly shaped by the legacy of a massive supernova progenitor. This association anchors the CCO, and therefore Vela Jr SNR, to the *Gaia* parallax distance of Ve 7–27, yielding a revised distance of 1.41 ± 0.14 kpc.

4. DISCUSSION

4.1. Physical Properties of Vela Jr at the Revised Distance

Placing Vela Jr at a distance of 1.41 ± 0.14 kpc through its association with Ve 7–27 (Figure 1) resolves long-standing inconsistencies that have complicated the interpretation of the remnant’s physical properties. With an angular radius of $0.95 \pm 0.02^\circ$ (Camilloni et al. 2023), Vela Jr’s physical radius becomes 23.3 ± 2.3 pc, which places Vela Jr in line with other Galactic SNRs of comparable radio surface brightness (Duncan & Green 2000).

The only observational constraint on Vela Jr’s shock motion comes from proper motion studies of its north-

western rim, which report expansion rates of $0.84 \pm 0.23 \text{ arcsec yr}^{-1}$ (Katsuda et al. 2008) and $0.42 \pm 0.10 \text{ arcsec yr}^{-1}$ (Allen et al. 2015). At the revised distance, these translate to shock velocities of $(5.6 \pm 1.5) \times 10^3 \text{ km s}^{-1}$ and $(2.8 \pm 0.7) \times 10^3 \text{ km s}^{-1}$, respectively. Assuming Sedov-Taylor evolution and $v = \frac{2}{5}R/t$, the inferred shock velocities imply ages of ~ 1.6 kyr and ~ 3.3 kyr. These values are in good agreement with the 2.4–5.1 kyr age range inferred by Allen et al. (2015) from hydrodynamical modeling and assuming expansion into a uniform ambient medium.

Combining these ages with the Sedov-Taylor scaling relation, $R_s \simeq 12.4 \text{ pc } (E_{51}/n)^{0.2} t_4^{0.4}$, where R_s is the remnant’s radius, E_{51} is the explosion energy in units of 10^{51} ergs, n the ambient density, and t_4 is the age in units of 10 kyr, we find $(E_{51}/n) \sim 9 \times 10^2$ for $t \sim 1.6$ kyr and $(E_{51}/n) \sim 2 \times 10^2$ for $t \sim 3.3$ kyr. For a canonical explosion energy of $E_{51} \sim 1$, these values imply very low ambient densities of $n \sim 10^{-3} - 5 \times 10^{-3} \text{ cm}^{-3}$ – consistent with expansion into a highly rarefied medium, such as a wind-blown cavity produced by a massive star progenitor. The inferred low ambient density explains the lack of strong thermal X-ray emission in Vela Jr as well as the high inferred velocity from a few kyr-old remnant.

The revised distance also substantially increases the remnant’s inferred very-high-energy γ -ray luminosity, $L_\gamma(1 - 10 \text{ TeV})$, from $3 \times 10^{32} \text{ erg s}^{-1}$ (Aharonian et al. 2005, ; that assumed a distance of 200 pc) to $1.5 \times 10^{34} \text{ erg s}^{-1}$, placing Vela Jr among the most luminous TeV-bright SNRs of comparable age. The corresponding total cosmic-ray proton energy above 1 GeV rises to $W_p \approx 5.1 \times 10^{48} \text{ erg}$, based on the scaling of

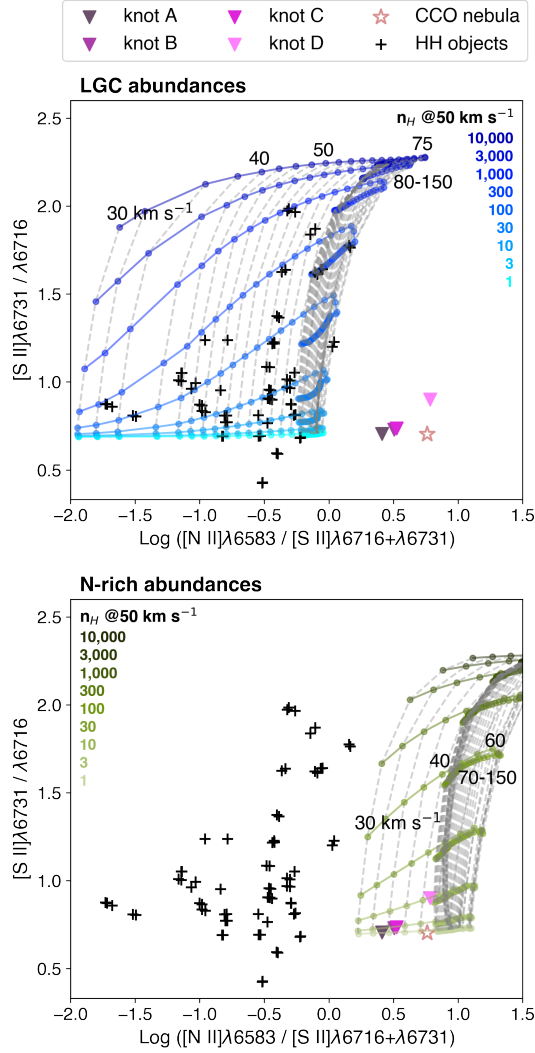


Figure 5. Line-ratio diagnostic diagram of $[S II]\lambda 6716 / \lambda 6731$ versus $[N II]\lambda 6583 / [S II]\lambda 6716 + \lambda 6731$, comparing MUSE measurements with slow-shock model prediction, computed with Local Galactic Concordance (LGC) abundances in blue lines (top) and nitrogen-rich (WN-like) abundances from Suherli et al. (2024) in green lines (bottom). Each panel shows the predicted values for shock velocities of 30–150 km s^{-1} and pre-shock hydrogen densities spanning $n_H = 1\text{--}10^4 \text{ cm}^{-3}$. Black ‘+’ symbols mark the classical HH objects from (Raga et al. 1996) and the inverted colored triangles represent HH knots A–D of Ve 7–27 (as labeled in Figure 2). The hollow red star denotes the CCO nebula; it is shown only for reference, as its emission is thought to arise from photoionization rather than shocks.

Fukui et al. 2024, emphasizing Vela Jr as an efficient cosmic-ray accelerator.

The implications extend further to the Vela Jr CCO, which plays an important role in the study of the dense matter nuclear equation of state (see, e.g., Potekhin

et al. 2015). At a distance of 750 pc, the inferred CCO’s X-ray luminosity is $\sim(1\text{--}2)\times 10^{32} \text{ erg s}^{-1}$ (Kargaltsev et al. 2002; Wu et al. 2021), low enough at a presumed young age (2–5 kyr) to indicate rapid cooling via the direct Urca neutrino emission that is only predicted to occur in high mass neutron stars for certain equations of state (Lattimer et al. 1991). Now with almost twice as large a distance, the higher CCO luminosity is still lower than neutron stars with canonical mass that cool slowly (Ho et al., in prep.). The larger distance also increases the possibility that the CCO has a carbon surface, inferred from modeling of the CCO X-ray spectrum (Potekhin et al. 2020; Wu et al. 2021; Alford & Halpern 2023), although a carbon composition is still unlikely due to the CCO age (Wijngaarden et al. 2019).

4.2. Linking Birth and Death

Protostellar lifetimes ($\sim 0.1\text{--}0.5 \text{ Myr}$; Evans et al. 2009) and HH flow dynamical ages ($10^4\text{--}10^5 \text{ yr}$; Reipurth & Bally 2001) exceed the few-kyr age inferred for Vela Jr, implying that Ve 7–27 must have formed well before the supernova explosion. Hydrodynamic simulations demonstrated that young stars and their protoplanetary disks can survive the blast wave of a nearby supernova, down to separations of a few tenths of a parsec, with significant stripping of the outer disks occurring only when the explosion is within $\lesssim 0.1 \text{ pc}$ (Ouellette et al. 2010, and references therein). At the revised distance, the projected $22''$ separation between Ve 7–27 and the Vela Jr CCO corresponds to $\sim 0.15 \text{ pc}$, which is in a range where disks are expected to survive, bearing in mind that the true distance is almost certainly greater than the projected value. Thus, a system such as Ve 7–27 could plausibly survive the Vela Jr supernova explosion.

The progenitor’s WN wind created a nitrogen-rich, oxygen-poor environment, and the subsequent core-collapse explosion enriched the same region with Fe-peak material. These abundance patterns observed in both Ve 7–27 and in the CCO nebula (Figures 3 and 4b,c) indicate that Ve 7–27 system resides within the chemically-enriched medium produced by the massive progenitor of Vela Jr during its final evolutionary stages.

The relatively small Doppler velocities observed in both the CCO nebula and the Ve 7–27 jet knots (Figure 4a) further support this picture. For HH objects to produce observable emission, their jets must collide with ambient material dense enough to generate radiative shocks. Such conditions arise naturally in the late WN phase, when the winds become increasingly clumpy and their velocities decline from thousands of km s^{-1} to only

a few tens of km s^{-1} near core collapse (Crowther 2007; see evolutionary models by Roy et al. 2021). This slow, nitrogen-rich material provides an ideal environment for producing the modest jet velocities observed and for sustaining the strong shock-excited emission from the knots and cocoon.

5. CONCLUSIONS

Accurately determining distances to Galactic supernova remnants remains a fundamental challenge, particularly for systems dominated by non-thermal emission. In Vela Jr, the chemical, spatial, and kinematic link between the CCO nebula and Ve 7–27 provides the first evidence of a YSO co-evolving within supernova-processed material. The Gaia parallax of Ve 7–27 therefore provides a direct geometric distance to the Vela Jr SNR, resolving the long-standing distance ambiguity for this enigmatic remnant and enabling a substantial revision of its physical properties.

The key results of this study are as follows:

- Ve 7–27 is a Young Stellar Object driving a bipolar Herbig-Haro outflow, located within the central $\sim 2'$ of the Vela Jr Supernova Remnant.
- Ve 7–27 and the Vela Jr CCO nebula share similar abundance signatures of unusually strong nitrogen enrichment and Fe-peak enhancement, confirming that they occupy the same chemically processed environment rather than a chance alignment.
- This association places Vela Jr at the distance of 1.41 ± 0.14 kpc, resolving decades of inconsistent distance estimates.
- At this distance, Vela Jr has a physical radius of 23.3 ± 2.3 pc and an age of ~ 1.6 – 3.3 kyr, based on the proper motion measurements of the north-western rim. Its large radius, high shock velocities, and very low inferred ambient density together indicate expansion into a wind-blown cavity carved by a massive progenitor. This naturally explains the remnant’s lack of strong thermal X-ray emission and the high blast wave velocity inferred for a 2–3 kyr old remnant dominated by non-thermal X-ray emission – further highlighting Vela Jr’s importance as a bright gamma-ray source and efficient particle accelerator.

These findings present a coherent picture of Vela Jr as a rapidly expanding SNR evolving within a low-density cavity, whose central region is interacting with an unusually enriched HH outflow, providing a rare, direct view

of how an SNR can influence nearby young stellar activity. Further optical and infrared spectroscopy, particularly with *James Webb Space Telescope* (JWST), will refine the abundance measurements of the Fe-peak elements and further constrain the excitation mechanisms in this unique environment. *Imaging X-ray Polarimetry Explorer* (IXPE) observations will shed light on the magnetic field geometry in the fast moving shocks and the processes for efficient particle acceleration in this non-thermal dominated SNR. Upcoming high-energy facilities such as the *Advanced X-ray Imaging Satellite* (AXIS; Reynolds et al. 2023; Safi-Harb et al. 2023) and the *Southern Wide-Field Gamma-ray Observatory* (SWGO; Albert et al. 2019) will provide powerful new constraints on shock physics, particle acceleration, and the complex environments that govern the evolution of Vela Jr and similar SNRs.

ACKNOWLEDGMENTS

We thank G. Ferrand for insightful discussions on visualization and SNR evolutionary scenarios. We also thank the anonymous referee for their careful review and valuable suggestions. This research made use of NASA’s ADS and SNRcat, the high-energy catalog of supernova remnants (<http://snrcat.physics.umanitoba.ca>). J.S. and S.S.H. acknowledge support from the Natural Sciences and Engineering Research Council of Canada (NSERC) through the Discovery Grants and the Canada Research Chairs programs. A.J.R. acknowledges funding support from the Australian Research Council, Future Fellowship award FT170100243. C-J.L. is supported by the NSTC grant 114-2112-M-004-001-MY2 from the National Science and Technology Council of Taiwan. R.M.C. acknowledges funding from the Australian Research Council under grant DP230101055.

AUTHOR CONTRIBUTIONS

J.S. led the project, performed the data analysis and modeling, and wrote most of the text. I.R.S. and S.S.H. provided scientific guidance and contributed to the interpretation of the results and editing of the manuscript. F.P.A.V. led the MUSE observing proposal and acquired the data presented in this study. All authors contributed to the discussion of the results and reviewed the manuscript.

Facility: VLT:Yepun (MUSE)

Software: SCIPY (Virtanen et al. 2020), ASTROPY (Astropy Collaboration et al. 2013, 2018, 2022), BRUTIFUS (Vogt 2019) (a Python module to process dat-

acubes from integral field spectrographs, that relies on STATSMODEL (Seabold & Perktold 2010), MATPLOTLIB, ASTROPY, and PHOTUTILS, an affiliated package of AS-

TROPY for photometry), MATPLOTLIB (Hunter 2007) (including the CUBEHELIX colormap (Green 2011)), and COSMOSCANVAS (English et al. 2024).

APPENDIX

A. PUBLISHED DISTANCE ESTIMATES FOR VELA JR

Early distance estimates for Vela Jr relied on X-ray surface brightness (Aschenbach 1998) and a detection of excess ^{44}Ti γ -ray emission (Iyudin et al. 1998; Aschenbach et al. 1999), which implied an exceptionally young and nearby remnant at 200–500 pc. Such proximity would require implausibly small physical dimensions and was inconsistent with the remnant’s unusually low radio surface brightness, placing it well below the empirical Σ – D relation for Galactic SNRs (Duncan & Green 2000). Later work showed that the reported ^{44}Ti feature was weak and ambiguous, making it unreliable as a distance indicator (Renaud et al. 2006; Weinberger et al. 2020). More recent constraints come on X-ray absorption modeling or shock expansion measurements (Slane et al. 2001; Katsuda et al. 2008; Acero et al. 2013; Allen et al. 2015) favor a larger distance but are inherently model-dependent and remain sensitive to assumptions about foreground absorption, ambient density, and explosion energy. In addition, Vela Jr’s position in a crowded and complex region complicates the separation of its emission components, particularly in radio and X-ray analyses. As a result, most existing distance estimates rely on indirect diagnostics tied to specific model assumptions and often focus on the bright northwestern rim, which may not represent the remnant as a whole.

Attempts to use the CCO as a distance anchor for Vela Jr have yielded no definitive result. *Chandra* proper motion measurements remain inconclusive due to the scarcity of suitable background reference sources, and a two-epoch comparison shows no significant displacement, implying a proper motion statistically consistent with zero (Mignani et al. 2019; Camilloni et al. 2023). This reinforces the view that the CCO remains near its birth site at the geometric center of the remnant. An indirect estimate of 2.4 ± 0.4 kpc (Reynoso et al. 2006) based on X-ray absorption modeling depends strongly on assumptions about Galactic gas distribution and therefore cannot robustly fix the distance.

B. MUSE DATA

A detailed description of the MUSE Wide Field Mode (WFM) program (Program ID 0104.D-0092(B); P.I.: F.P.A. Vogt), data reduction, calibrations, and post-processing sequences, is provided in Section 2 of Suherli et al. (2024). While the earlier publication focused on a $10'' \times 10''$ region centered on the CCO, in this work we use the full field of the final datacube. The complete mosaic spans 607×623 spaxels, corresponding to an area of approximately $121.4'' \times 124.6''$ on the sky, at the MUSE spatial sampling of $0.2''$ spaxel $^{-1}$.

C. EMISSION-LINE FITTING AND VELOCITY CHANNEL MAPS

To derive the kinematic and line-ratio maps presented in this work, we performed a spaxel-by-spaxel multi-Gaussian fit to the prominent optical emission lines within the CCO Nebula and Ve 7–27 HH outflow region of the MUSE datacube. The analysis was carried out using a dedicated PYTHON workflow that applies single- and two-component Gaussian fits, optimized with a non-linear least squares fitter (SCIPY’s CURVE_FIT function), to $\text{H}\alpha$, $[\text{N II}]\lambda\lambda 6548, 6583$ doublet (with the theoretical 1:3 flux ratio enforced), and $[\text{S II}]\lambda\lambda 6716, 6731$ doublet. Two-component fits were attempted only when the single-component model failed to provide an adequate fit of the spectrum, otherwise, spaxels defaulted to a single-component solution. Instrumental broadening at each wavelength was determined from the MUSE line-spread function provided by BRUTIFUS (Vogt 2019), and the instrumental σ was adopted as the lower bound for all the fitted line widths.

In addition to the spaxel-by-spaxel analysis, we extracted integrated spectra for knots A–D and for the CCO nebula, as indicated in Figure 2. Each spectrum was obtained by summing over a 7×4 spaxel region centered on the peak-brightness spaxel of each feature. The integrated spectra were fitted using simultaneous two-component Gaussian models for the $\text{H}\alpha$, $[\text{N II}]\lambda\lambda 6548, 6583$, and $[\text{S II}]\lambda\lambda 6716, 6731$ emission lines. Line fitting was carried out using a custom PYTHON code that implements the SCIPY’s CURVE_FIT function, which minimizes the residuals between the observed line profiles and the model. Simultaneously fitting all five lines provides robust measurements of the line fluxes and Doppler velocities of both Gaussian components. From the fitted fluxes, we computed the $[\text{N II}]/\text{H}\alpha$ and $[\text{N II}]/[\text{S II}]$ ratios, which serves as an indicator of nitrogen enrichment, as well as the $[\text{S II}]\lambda 6731/\lambda 6716$ ratio.

Channel maps are two-dimensional images that isolate emission within specific velocity intervals along the line of sight, allowing for the spatial distribution of gas at different radial velocities to be visualized. We constructed channel maps of H α (red), [N II] λ 6583 (green), and [Ni II] λ 7378 (blue) emission (Figure 6) from the continuum-subtracted MUSE datacube.

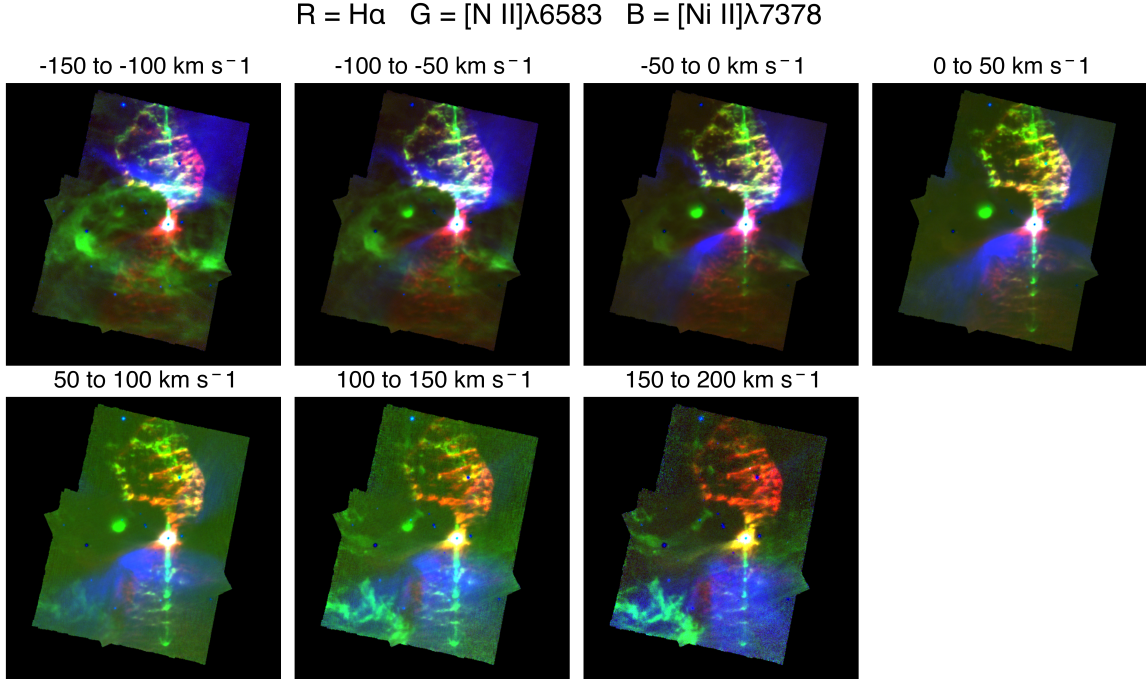


Figure 6. Channel maps of H α (red), [N II] λ 6583 (green), and [Ni II] λ 7378 (blue) emission from the continuum-subtracted MUSE datacube, from -150 to $+200$ km s $^{-1}$. Each panel shows the integrated intensity within a fixed velocity slice indicated in the label. The red square marks the CCO nebula.

D. SHOCK MODELING WITH MAPPINGS

We performed slow-shock modeling using MAPPINGS v5.2.0 (Sutherland et al. 2018), considering both standard ISM (Local Galactic Concordance, LGC) abundances (Nicholls et al. 2017) and nitrogen-rich abundances of WN star evolution (as adopted in Suherli et al. 2024), over a velocity range of 30 to 250 km s $^{-1}$ in increments of 2.5 km s $^{-1}$, using a fixed shock ram pressure to eliminate the velocity dependence on surface brightness. The ram pressure is normalized relative to the pre-shock hydrogen number density at a shock velocity at 50 km s $^{-1}$. Constant-pressure conditions were modeled over the entire velocity range for pre-shock hydrogen densities (n_H) of 1, 3, 10, 30, 100, 300, 1000, 3000, and 10,000 cm $^{-3}$.

E. TOTAL ENERGY (IN COSMIC-RAY PROTONS) APPROXIMATION

In hadronic models, where γ -rays arise from collisions between shock-accelerated protons and ambient gas, the γ -ray luminosity L_γ is governed by the total energy in cosmic-ray protons (W_p) and the proton-proton collision timescale (t_{pp}), such that $L_\gamma \propto W_p/t_{pp}$. Here, t_{pp} is inversely proportional to the ambient hydrogen density n_H . The ambient density can be approximated by $n_H \approx N_H/\Delta D$, where N_H is the hydrogen column density and ΔD is the physical path length through the emitting region. To the extent that we can ignore other gas along the line of sight, the N_H is a measured quantity, and given we can reasonably adopt that $\Delta D \propto d$ at fixed angular size, therefore the collision timescale scales with distance as $t_{pp} \propto 1/n_H \propto \Delta D/N_H \propto d$.

Given that $L_\gamma \propto d^2 F_\gamma$, we can derive the scaling relation for W_p as $L_\gamma \propto W_p/d \implies W_p \propto d^3$. With this cubic dependence on distance, the revised distance of 1.41 kpc implies that Vela Jr's total CR proton energy is a factor of $(1.41/0.75)^3 \approx 6.6$ higher than previously estimated. This raises the inferred W_p from 7.7×10^{47} erg (for >1 GeV cosmic ray protons), assuming $d = 0.75$ kpc and $n_H = 90$ cm $^{-3}$ (Fukui et al. 2024), to roughly 5.1×10^{48} erg, exceeding

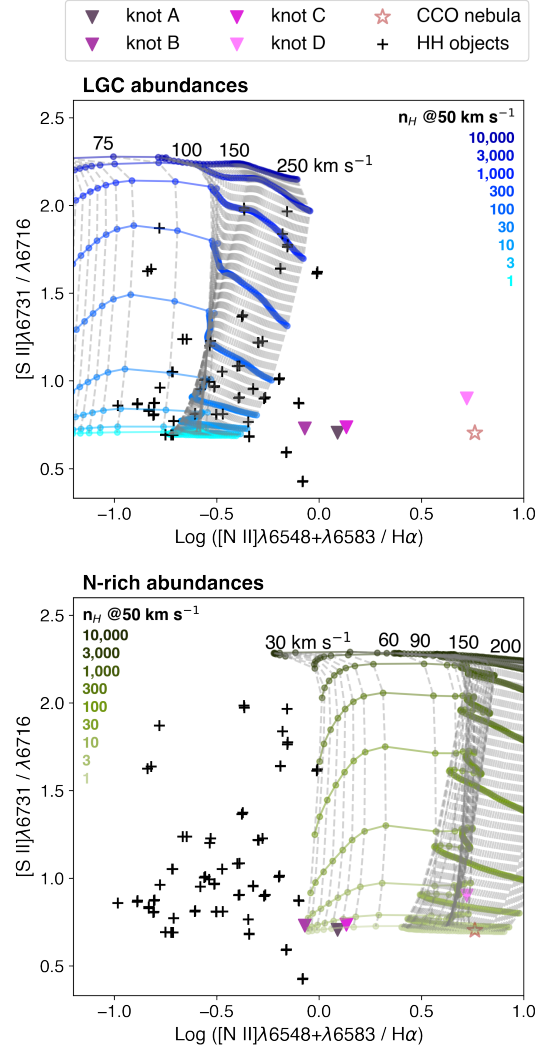


Figure 7. Line-ratio diagnostic diagram of $[S II]\lambda 6716 / \lambda 6731$ versus $[N II]\lambda 6548 + \lambda 6583 / H\alpha$, comparing MUSE measurements with slow-shock model prediction, computed with Local Galactic Concordance (LGC) abundances in blue lines (top) and nitrogen-rich (WN-like) abundances from Suherli et al. (2024) in green lines (bottom). Each panel shows the predicted values for shock velocities of 30–250 km s^{-1} and pre-shock hydrogen densities spanning $n_H = 1 - 10^4 \text{ cm}^{-3}$. Black ‘+’ symbols mark the classical HH objects from (Raga et al. 1996) and the inverted colored triangles represent HH knots A–D of Ve 7–27 (as labeled in Figure 2). The hollow the red star denotes the CCO nebula; it is shown only for reference, as its emission is thought to arise from photoionization rather than shocks.

the value estimated for RX J1713.7–3946 by at least a factor of five. This suggests that Vela Jr is one of the most powerful Galactic cosmic-ray accelerators among known Galactic SNRs

REFERENCES

- Abbott, R., Abbott, T. D., Acernese, F., et al. 2022, *PhRvD*, 105, 082005, doi: [10.1103/PhysRevD.105.082005](https://doi.org/10.1103/PhysRevD.105.082005)
- Acero, F., Gallant, Y., Ballet, J., Renaud, M., & Terrier, R. 2013, *A&A*, 551, A7, doi: [10.1051/0004-6361/201220799](https://doi.org/10.1051/0004-6361/201220799)
- Aharonian, F., Akhperjanian, A. G., Bazer-Bachi, A. R., et al. 2005, *Å*, 437, L7, doi: [10.1051/0004-6361:200500130](https://doi.org/10.1051/0004-6361:200500130)
- . 2007, *ApJ*, 661, 236, doi: [10.1086/512603](https://doi.org/10.1086/512603)
- Albert, A., Alfaro, R., Ashkar, H., et al. 2019, arXiv e-prints, arXiv:1902.08429, doi: [10.48550/arXiv.1902.08429](https://doi.org/10.48550/arXiv.1902.08429)
- Alford, J. A. J., & Halpern, J. P. 2023, *ApJ*, 944, 36, doi: [10.3847/1538-4357/acaf55](https://doi.org/10.3847/1538-4357/acaf55)

- Allen, D. A., & Glass, I. S. 1975, *MNRAS*, 170, 579, doi: [10.1093/mnras/170.3.579](https://doi.org/10.1093/mnras/170.3.579)
- Allen, G. E., Chow, K., DeLaney, T., et al. 2015, *ApJ*, 798, 82, doi: [10.1088/0004-637X/798/2/82](https://doi.org/10.1088/0004-637X/798/2/82)
- Aschenbach, B. 1998, *Nature*, 396, 141, doi: [10.1038/24103](https://doi.org/10.1038/24103)
- Aschenbach, B., Iyudin, A. F., & Schönfelder, V. 1999, *Å*, 350, 997, doi: [10.48550/arXiv.astro-ph/9909415](https://doi.org/10.48550/arXiv.astro-ph/9909415)
- Astropy Collaboration, Robitaille, T. P., Tollerud, E. J., et al. 2013, *A&A*, 558, A33, doi: [10.1051/0004-6361/201322068](https://doi.org/10.1051/0004-6361/201322068)
- Astropy Collaboration, Price-Whelan, A. M., Sipőcz, B. M., et al. 2018, *AJ*, 156, 123, doi: [10.3847/1538-3881/aabc4f](https://doi.org/10.3847/1538-3881/aabc4f)
- Astropy Collaboration, Price-Whelan, A. M., Lim, P. L., et al. 2022, *ApJ*, 935, 167, doi: [10.3847/1538-4357/ac7c74](https://doi.org/10.3847/1538-4357/ac7c74)
- Bacon, R., Accardo, M., Adjali, L., et al. 2010, in *Society of Photo-Optical Instrumentation Engineers (SPIE) Conference Series*, Vol. 7735, *Ground-based and Airborne Instrumentation for Astronomy III*, ed. I. S. McLean, S. K. Ramsay, & H. Takami, 773508, doi: [10.1117/12.856027](https://doi.org/10.1117/12.856027)
- Bally, J. 2016, *ARA&A*, 54, 491, doi: [10.1146/annurev-astro-081915-023341](https://doi.org/10.1146/annurev-astro-081915-023341)
- Camilloni, F., Becker, W., Predehl, P., et al. 2023, *Å*, 673, A45, doi: [10.1051/0004-6361/202245475](https://doi.org/10.1051/0004-6361/202245475)
- Crowther, P. A. 2007, *ARA&A*, 45, 177, doi: [10.1146/annurev.astro.45.051806.110615](https://doi.org/10.1146/annurev.astro.45.051806.110615)
- De Luca, A. 2017, in *Journal of Physics Conference Series*, Vol. 932, *Journal of Physics Conference Series (IOP)*, 012006, doi: [10.1088/1742-6596/932/1/012006](https://doi.org/10.1088/1742-6596/932/1/012006)
- Dopita, M. A., & Sutherland, R. S. 2017, *ApJS*, 229, 35, doi: [10.3847/1538-4365/aa6542](https://doi.org/10.3847/1538-4365/aa6542)
- Duncan, A. R., & Green, D. A. 2000, *Å*, 364, 732, doi: [10.48550/arXiv.astro-ph/0009289](https://doi.org/10.48550/arXiv.astro-ph/0009289)
- English, J., Richardson, M. L. A., Ferrand, G., & Deg, N. 2024, *CosmosCanvas: Useful color maps for different astrophysical properties*, *Astrophysics Source Code Library*, record ascl:2401.005. <http://ascl.net/2401.005>
- Evans, II, N. J., Dunham, M. M., Jørgensen, J. K., et al. 2009, *ApJS*, 181, 321, doi: [10.1088/0067-0049/181/2/321](https://doi.org/10.1088/0067-0049/181/2/321)
- Ferrand, G., & Safi-Harb, S. 2012, *Advances in Space Research*, 49, 1313, doi: [10.1016/j.asr.2012.02.004](https://doi.org/10.1016/j.asr.2012.02.004)
- Fukui, Y., Aruga, M., Sano, H., et al. 2024, *ApJ*, 961, 162, doi: [10.3847/1538-4357/ad0da3](https://doi.org/10.3847/1538-4357/ad0da3)
- Fukui, Y., Sano, H., Sato, J., et al. 2017, *ApJ*, 850, 71, doi: [10.3847/1538-4357/aa9219](https://doi.org/10.3847/1538-4357/aa9219)
- Gaia Collaboration, Brown, A. G. A., Vallenari, A., et al. 2021, *A&A*, 649, A1, doi: [10.1051/0004-6361/202039657](https://doi.org/10.1051/0004-6361/202039657)
- Green, D. A. 2011, *Bulletin of the Astronomical Society of India*, 39, 289, doi: [10.48550/arXiv.1108.5083](https://doi.org/10.48550/arXiv.1108.5083)
- H. E. S. S. Collaboration, Abdalla, H., Abramowski, A., et al. 2018, *Å*, 612, A7, doi: [10.1051/0004-6361/201630002](https://doi.org/10.1051/0004-6361/201630002)
- Hunter, J. D. 2007, *Computing in Science & Engineering*, 9, 90, doi: [10.1109/MCSE.2007.55](https://doi.org/10.1109/MCSE.2007.55)
- Iyudin, A. F., Schönfelder, V., Bennett, K., et al. 1998, *Nature*, 396, 142, doi: [10.1038/24106](https://doi.org/10.1038/24106)
- Kargaltsev, O., Pavlov, G. G., Sanwal, D., & Garmire, G. P. 2002, *ApJ*, 580, 1060, doi: [10.1086/343852](https://doi.org/10.1086/343852)
- Katsuda, S., Tsunemi, H., & Mori, K. 2008, *ApJL*, 678, L35, doi: [10.1086/588499](https://doi.org/10.1086/588499)
- Landaberry, S. J. C., Pereira, C. B., & de Araújo, F. X. 2001, *A&A*, 376, 917, doi: [10.1051/0004-6361:20010947](https://doi.org/10.1051/0004-6361:20010947)
- Lattimer, J. M., Pethick, C. J., Prakash, M., & Haensel, P. 1991, *PhRvL*, 66, 2701, doi: [10.1103/PhysRevLett.66.2701](https://doi.org/10.1103/PhysRevLett.66.2701)
- Mignani, R. P., de Luca, A., Zaggia, S., et al. 2007, *Å*, 473, 883, doi: [10.1051/0004-6361:20077768](https://doi.org/10.1051/0004-6361:20077768)
- Mignani, R. P., De Luca, A., Zharikov, S., et al. 2019, *MNRAS*, 486, 5716, doi: [10.1093/mnras/stz1195](https://doi.org/10.1093/mnras/stz1195)
- Ming, J., Papa, M. A., Eggenstein, H. B., et al. 2024, *ApJ*, 977, 154, doi: [10.3847/1538-4357/ad8b9e](https://doi.org/10.3847/1538-4357/ad8b9e)
- Nicholls, D. C., Sutherland, R. S., Dopita, M. A., Kewley, L. J., & Groves, B. A. 2017, *MNRAS*, 466, 4403, doi: [10.1093/mnras/stw3235](https://doi.org/10.1093/mnras/stw3235)
- Ouellette, N., Desch, S. J., & Hester, J. J. 2010, *ApJ*, 711, 597, doi: [10.1088/0004-637X/711/2/597](https://doi.org/10.1088/0004-637X/711/2/597)
- Pavlov, G. G., Sanwal, D., Kızıltan, B., & Garmire, G. P. 2001, *ApJL*, 559, L131, doi: [10.1086/323975](https://doi.org/10.1086/323975)
- Pellizzoni, A., Mereghetti, S., & De Luca, A. 2002, *Å*, 393, L65, doi: [10.1051/0004-6361:20021207](https://doi.org/10.1051/0004-6361:20021207)
- Potekhin, A. Y., Pons, J. A., & Page, D. 2015, *SSRv*, 191, 239, doi: [10.1007/s11214-015-0180-9](https://doi.org/10.1007/s11214-015-0180-9)
- Potekhin, A. Y., Zyuzin, D. A., Yakovlev, D. G., Beznogov, M. V., & Shibanov, Y. A. 2020, *MNRAS*, 496, 5052, doi: [10.1093/mnras/staa1871](https://doi.org/10.1093/mnras/staa1871)
- Raga, A. C., Böhm, K. H., & Cantó, J. 1996, *RMxAA*, 32, 161
- Reipurth, B., & Bally, J. 2001, *ARA&A*, 39, 403, doi: [10.1146/annurev.astro.39.1.403](https://doi.org/10.1146/annurev.astro.39.1.403)
- Renaud, M., Vink, J., Decourchelle, A., et al. 2006, *NewAR*, 50, 540, doi: [10.1016/j.newar.2006.06.061](https://doi.org/10.1016/j.newar.2006.06.061)
- Reynolds, C. S., Kara, E. A., Mushotzky, R. F., et al. 2023, in *Society of Photo-Optical Instrumentation Engineers (SPIE) Conference Series*, Vol. 12678, *UV, X-Ray, and Gamma-Ray Space Instrumentation for Astronomy XXIII*, ed. O. H. Siegmund & K. Hoadley, 126781E, doi: [10.1117/12.2677468](https://doi.org/10.1117/12.2677468)
- Reynolds, S. P. 2008, *ARA&A*, 46, 89, doi: [10.1146/annurev.astro.46.060407.145237](https://doi.org/10.1146/annurev.astro.46.060407.145237)

- Reynoso, E. M., Dubner, G., Giacani, E., Johnston, S., & Green, A. J. 2006, *Å*, 449, 243, doi: [10.1051/0004-6361:20054236](https://doi.org/10.1051/0004-6361:20054236)
- Roy, A., Dopita, M. A., Krumholz, M. R., et al. 2021, *MNRAS*, 502, 4359, doi: [10.1093/mnras/stab376](https://doi.org/10.1093/mnras/stab376)
- Roy, A., Sutherland, R. S., Krumholz, M. R., Heger, A., & Dopita, M. A. 2020, *MNRAS*, 494, 3861, doi: [10.1093/mnras/staa781](https://doi.org/10.1093/mnras/staa781)
- Safi-Harb, S., Burdge, K. B., Bodaghee, A., et al. 2023, arXiv e-prints, arXiv:2311.07673, doi: [10.48550/arXiv.2311.07673](https://doi.org/10.48550/arXiv.2311.07673)
- Seabold, S., & Perktold, J. 2010, in 9th Python in Science Conference
- Slane, P., Hughes, J. P., Edgar, R. J., et al. 2001, *ApJ*, 548, 814, doi: [10.1086/319033](https://doi.org/10.1086/319033)
- Suherli, J., Safi-Harb, S., Seitzzahl, I. R., et al. 2024, *MNRAS*, 527, 9263, doi: [10.1093/mnras/stad3740](https://doi.org/10.1093/mnras/stad3740)
- Sutherland, R., Dopita, M., Binette, L., & Groves, B. 2018, MAPPINGS V: Astrophysical plasma modeling code, Astrophysics Source Code Library, record ascl:1807.005. <http://ascl.net/1807.005>
- Tananbaum, H. 1999, *IAUC*, 7246, 1
- Velghe, A. G. 1957, *ApJ*, 126, 302, doi: [10.1086/146401](https://doi.org/10.1086/146401)
- Virtanen, P., Gommers, R., Oliphant, T. E., et al. 2020, *Nature Methods*, 17, 261, doi: [10.1038/s41592-019-0686-2](https://doi.org/10.1038/s41592-019-0686-2)
- Vogt, F. P. A. 2019, brutifus: Python module to post-process datacubes from integral field spectrographs, Astrophysics Source Code Library, record ascl:1903.004. <http://ascl.net/1903.004>
- Weinberger, C., Diehl, R., Pleintinger, M. M. M., Siegert, T., & Greiner, J. 2020, *Å*, 638, A83, doi: [10.1051/0004-6361/202037536](https://doi.org/10.1051/0004-6361/202037536)
- Wijngaarden, M. J. P., Ho, W. C. G., Chang, P., et al. 2019, *MNRAS*, 484, 974, doi: [10.1093/mnras/stz042](https://doi.org/10.1093/mnras/stz042)
- Wray, J. D. 1966, PhD thesis, Northwestern University
- Wu, Q., Pires, A. M., Schwobe, A., et al. 2021, *Research in Astronomy and Astrophysics*, 21, 294, doi: [10.1088/1674-4527/21/11/294](https://doi.org/10.1088/1674-4527/21/11/294)